Reduction of Current Harmonics in Grid-Connected PV Inverters using Harmonic Compensation - Conforming to IEEE and IEC Standards

Daniel Zammit, Cyril Spiteri Staines, Maurice Apap

Department of Industrial Electrical Power Conversion, Faculty of Engineering, University of Malta, Msida, MSD 2080, Malta

Corresponding author: daniel.zammit@um.edu.mt

Abstract. This paper deals with the reduction of harmonics generated by Grid-Connected PV Inverters to conform to the harmonic limits set by the IEEE and IEC standards. An analysis of the current harmonics present in the output current of a grid-connected inverter will be presented. The inverter will be current controlled by a Proportional-Resonant (PR) current controller. The design and testing of the PR current controller will be presented. This paper will also deal with the application of harmonic compensation to make the inverter compliant to the standards, by using selective harmonic compensators in addition to the Proportional-Resonant (PR) controller. Both simulation and experimental results will be presented. Testing was carried out on a Grid-Connected PV Inverter which was designed and constructed for this research.

Keywords. Inverters; Proportional-Resonant Controllers; Harmonic Compensation; Photovoltaic.

1. Introduction

Distributed power generation systems connected to the electricity supply grid are always increasing, especially inverter based renewable energy generation systems. This high penetration of inverter based power generation systems can cause a power quality issue due to the harmonics injected into the supply grid. This means that it is very important to control the harmonics generated by these inverters to limit their adverse effects on the grid power quality. IEEE and European IEC standards suggest harmonic limits generated by Photovoltaic (PV) Systems and Distributed Power Resources for the current total harmonic distortion (THD) factor and also for the magnitude of each harmonic. The IEEE 929 and IEEE 1547 standards allow a limit of 4% for each harmonic from 3^{rd} to 9^{th} and 2% for 11^{th} to 15^{th} [1], [2]. The IEC 61727 standard specifies similar limits [3].

In current-controlled PV inverters the current controller can have a significant effect on the quality of the current supplied to the grid by the inverter, and therefore it is important that the controller provides a high quality sinusoidal output with minimal distortion to avoid creating harmonics. A controller which is commonly used in current-controlled PV inverters is the Proportional-Resonant

(PR) controller. The performance of the PR controller has been discussed in a number of papers including [4-10] among others. Another type of current controller which can be used in grid-connected inverters is the Proportional-Integral (PI) controller, but this type of controller has the drawback of not being able to follow a sinusoidal reference without steady state error. On the other hand, the PR controller is more suited to operate with sinusoidal references, and does not suffer from steady state error issues. This makes the PR controller an ideal choice for grid-connected inverters. The PR controller has the ability to provide gain at a certain frequency (resonant frequency) and almost no gain exists at the other frequencies. Although the PR controller has a high ability to track a sinusoidal reference such as a current waveform, the output current of the grid-connected inverter is not immune from harmonic content [8]. Harmonics in the output current can result due to the converter non-linearities as well as from harmonics which are already present in the grid. Selective harmonics in the current can be compensated by using additional PR controllers which act at particular harmonic frequencies to be reduced or eliminated such as the 3^{rd}, 5^{th}, 7^{th} and so on. This compensation can be used to reduce the current THD and make the inverter compliant to the IEEE and IEC standards [4] [9] [10] [11].

This paper presents the design and analysis of the PR current controller. In addition to the fundamental PR current controller, selective harmonic compensators are designed and applied for the 3^{rd}, 5^{th} and 7^{th} harmonics, to make the inverter system compliant to the IEEE and IEC standards. The design of the current controller and harmonic compensators was carried out using Matlab's SISO Design Tool. Test results obtained by simulations and by experimental tests for the PR and the harmonic compensators will be presented. Experimental testing was carried out on a single phase 3kW grid-connected PV inverter, which was designed and built for this research. Figure 1 shows the block diagram of the Grid-Connected PV Inverter system connected to the grid through an LCL filter used for this research.

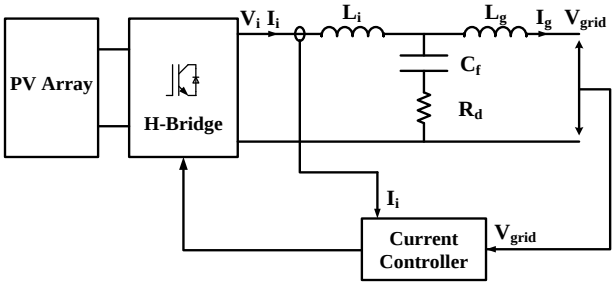

Figure 1. Block diagram of the Grid-Connected PV Inverter with the LCL Filter

This paper is divided into six sections. Section two covers the theory for the LCL filter, the PR current control, as well as the harmonic compensators. Section three covers the design of the LCL filter and the PR current controller including the harmonic compensators. Sections four and five present the simulations and inverter testing, respectively. A comparison of results of the current controllers is covered in section six. Section seven presents the final comments concluding the paper.

2. LCL Filter and Current Control

2.1. LCL Filter

The transfer function of the LCL filter of Figure 1 in terms of the inverter current I_i and the inverter voltage U_i, neglecting R_d, is:

$$G_F(s) = \frac{I_i}{U_i} = \frac{1}{L_i s} \frac{\left(s^2 + \left(\frac{1}{L_g C_f}\right)\right)}{\left(s^2 + \left(\frac{L_i + L_g}{L_i L_g C_f}\right)\right)} \quad (1)$$

where, L_i is the inverter side inductor
L_g is the grid side inductor
and C_f is the filter capacitor

The resonant frequency of the filter is given by:

$$\omega_{res} = \sqrt{\frac{(L_i + L_g)}{(L_i L_g C_f)}} \quad (2)$$

The transfer function in (1) does not include the damping resistor R_d. The introduction of R_d in series with the capacitor C_f increases stability and reduces resonance [12]. This method of damping is a type of passive damping. Whilst there exist other methods of passive damping and also more advanced active damping methods, this particular damping method used was considered enough for the aim and purpose of this research due to its simplicity. The transfer function of the filter taking in consideration the damping resistor R_d is:

$$G_F(s) = \frac{I_i}{U_i} = \frac{1}{L_i s} \frac{\left(s^2 + s\left(\frac{R_d}{L_g}\right) + \left(\frac{1}{L_g C_f}\right)\right)}{\left(s^2 + s\left(\frac{(L_i + L_g)R_d}{L_i L_g}\right) + \left(\frac{L_i + L_g}{L_i L_g C_f}\right)\right)} \quad (3)$$

2.2. PR Control

Figure 2 shows the PR current control strategy. I_i is the inverter output current, I_i^* is the inverter current reference and U_i^* is the inverter voltage reference.

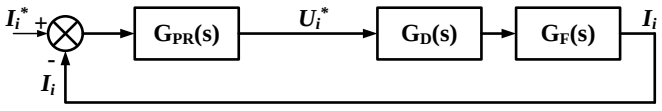

Figure 2. The PR Current Control

The PR current controller $G_{PR}(s)$ is represented by:

$$G_{PR}(s) = K_P + K_I \frac{s}{s^2 + {\omega_0}^2} \quad (4)$$

where, K_P is the Proportional Gain term, K_I is the Integral Gain term and ω_0 is the resonant frequency.

$G_F(s)$ represents the LCL filter. $G_D(s)$ represents the processing delay of the microcontroller, which is typically equal to the time of one sample T_s and is represented by:

$$G_D(s) = \frac{1}{1 + sT_s} \tag{5}$$

The ideal resonant term on its own in the PR controller provides an infinite gain at the ac frequency ω_0 and no phase shift and gain at the other frequencies [13]. The K_P term determines the dynamics of the system; bandwidth, phase and gain margins [13].

Equation (4) represents an ideal PR controller which can give stability problems because of the infinite gain. To avoid these problems, the PR controller can be made non-ideal by introducing damping as shown in (6).

$$G_{PR}(s) = K_P + K_I \frac{2\omega_c s}{s^2 + 2\omega_c s + {\omega_0}^2} \tag{6}$$

where, ω_c is the bandwidth around the ac frequency of ω_0.

With (6) the gain of the PR controller at the ac frequency ω_0 is now finite and it is still large enough to provide only a very small steady state error. This equation also makes the controller more easily realizable in digital systems due to their finite precision [7].

2.3. PR Control with Harmonic Compensators

Figure 3 below shows the PR current control with an additional harmonic compensation block $G_H(s)$.

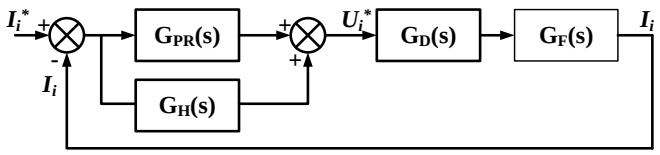

Figure 3. The PR Current Control with Harmonic Compensators

The harmonic compensator $G_H(s)$ is represented by:

$$G_H(s) = \sum_{h=3,5,7,\ldots} K_{Ih} \frac{s}{s^2 + (h\omega_0)^2} \tag{7}$$

where, K_{Ih} is the Resonant term at the particular harmonic and $h\omega_0$ is the resonant frequency of the particular harmonic.

The harmonic compensator for each harmonic frequency is added to the fundamental frequency PR controller to form the complete current controller, as shown in Figure 3.

Equation (7) represents an ideal harmonic compensator which as stated for the fundamental PR controller, can give stability problems due to the infinite gain. To avoid these problems, the harmonic compensator equation can be made non-ideal by representing it using (8).

$$G_H(s) = \sum_{h=3,5,7,\ldots} K_{Ih} \frac{2\omega_c s}{s^2 + 2\omega_c s + (h\omega_0)^2} \tag{8}$$

where, ω_c is the bandwidth around the particular harmonic frequency of $h\omega_0$.

As for the case of the fundamental PR controller, with (8) the gain of the harmonic compensator at the harmonic frequency $h\omega_0$ is now finite but it is still large enough to provide compensation.

3. LCL Filter, PR Controller and Harmonic Compensators Design

3.1. Inverter and LCL Filter Design Parameters

To carry out the tests using the PR control and the harmonic compensation, a 3kW Grid-Connected Inverter was designed and constructed. The LCL filter was designed following the procedure in [13] and [14]. Designing for a dc-link voltage of 358V, maximum ripple current of 20% of the grid peak current, a switching frequency of 10kHz, filter cut-off frequency of 2kHz and the capacitive reactive power not exceeding 5% of rated power, the following values of the LCL filter were obtained: L_i = 1.2mH, L_g = 0.7mH, C_f = 9μF and R_d = 8Ω.

3.2. PR Controller Design

The block diagram of the system used to design the control is shown in figure 2, with the only difference that an Anti-aliasing filter was introduced in the inverter current feedback path to prevent the aliasing effect when sampling the inverter current. The Anti-Aliasing filter used was a second order non-inverting active low pass filter using the Sallen-Key filter implementation and a Butterworth design with cut-off frequency of 2.5kHz.

The optimal fundamental PR current controller design was carried out using SISO Tool in Matlab. To design the optimal controller, the integral gain K_I at the ac frequency ω_0 must be set large enough to enforce only a very small steady state error, and also set the proportional gain K_P value to obtain sufficient bandwidth accommodating the other harmonic compensators which would otherwise cause system instability. The PR controller was designed for a resonant frequency ω_0 of 314.16rad/s (50Hz) and ω_c was set to be 0.5rad/s, obtaining a K_P of 6.8 and K_I of 1498.72, shown in (9).

$$G_{PR}(s) = 6.8 + 1498.72 \frac{s}{s^2 + s + (2\pi(50))^2} \tag{9}$$

Figure 4 shows the root locus plot in Matlab of the system including the LCL filter, the processing delay, anti-aliasing filter in the output current feedback path and the PR controller. The root locus plot shows that the designed system is stable.

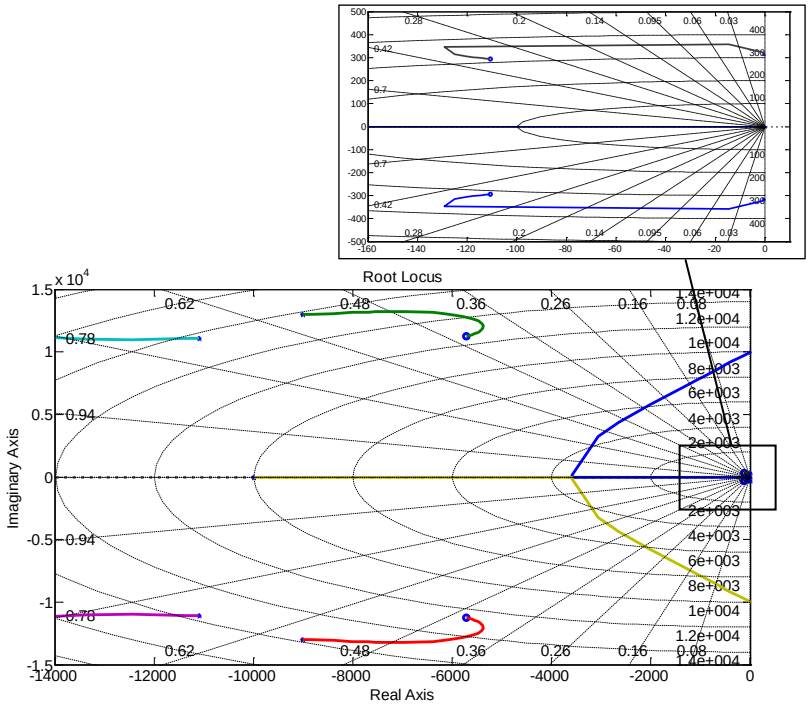

Figure 4. Root Locus of the Inverter with the PR Controller

Figure 5 and figure 6 show the open loop bode diagram and the closed loop bode diagram of the system, respectively. From the open loop bode diagram, the Gain Margin obtained is 13.9dB at a frequency of 9970rad/s and the Phase Margin obtained is 51deg at a frequency of 3300rad/s.

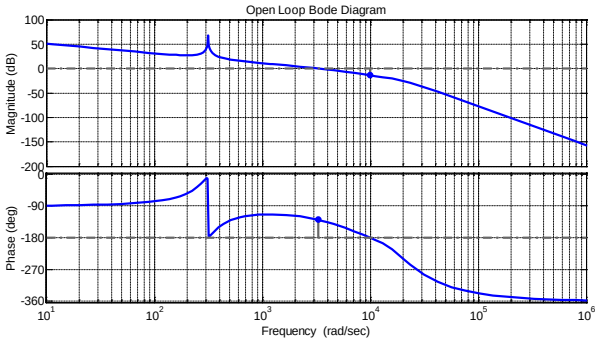

Figure 5. Open Loop Bode Diagram of the System with PR Control

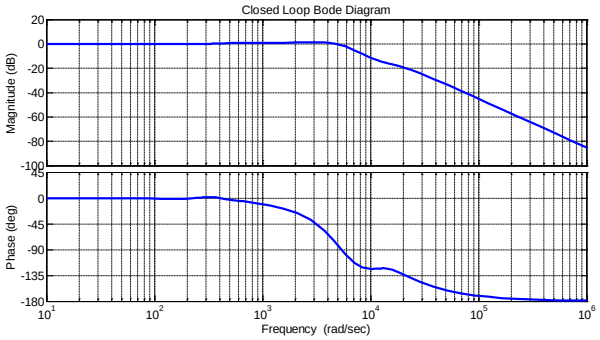

Figure 6. Closed Loop Bode Diagram of the System with PR Control

3.3. Harmonic Compensators Design

The block diagram of the complete system used to design the selective harmonic compensators is shown in figure 3. In the inverter current feedback path the same Anti-aliasing filter as the one used with the PR controller was used to prevent the aliasing effect when sampling the inverter current.

Harmonic compensators were designed for the 3rd, 5th and 7th harmonics. The PR harmonic compensators were designed using SISO Tool in Matlab with the resonant frequency set to the particular frequency to be compensated, i.e. 150Hz for the 3rd harmonic, 250Hz for the 5th harmonic and 350Hz for the 7th harmonic. Similarly to the fundamental PR current control design, the Root Locus, Open Loop and Closed Loop Bode diagrams plotted by SISO Tool were used to achieve the optimal design for each harmonic compensator. Each harmonic compensator was designed on its own and then combined together with the fundamental PR controller at the end in SISO Tool. Ultimately

fine tuning of the compensators was performed to obtain the optimum operation of the compensators by varying ω_c and K_I of the corresponding compensator. Care was taken that the system remains stable, by using the gain margin and phase margin stability criteria.

The 3rd harmonic compensator at a resonant frequency $3\omega_0$ of 942.48rad/s (150Hz) was designed with a ω_c of 2.5rad/s and a K_I of 211.208. The 5th harmonic compensator at a resonant frequency $5\omega_0$ of 1570.8rad/s (250Hz) was designed with a ω_c of 4.5rad/s and a K_I of 83.867. The 7th harmonic compensator at a resonant frequency $7\omega_0$ of 2199.11rad/s (350Hz) was designed with a ω_c of 10rad/s and a K_I of 40.834. The transfer function of the complete controller $G_C(s)$ is shown in (10).

$$G_C(s) = G_{PR}(s) + G_{3H}(s) + G_{5H}(s) + G_{7H}(s)$$

$$= \frac{6.8\left(s^2 + 221.4s + (2\pi \times 50)^2\right)}{s^2 + s + (2\pi \times 50)^2} + \frac{1056.04s}{s^2 + 5s + (2\pi \times 150)^2} + \frac{754.8s}{s^2 + 9s + (2\pi \times 250)^2} + \frac{816.68s}{s^2 + 20s + (2\pi \times 350)^2} \quad (10)$$

Figure 7 shows the root locus plot in Matlab of the system with the additional harmonic compensators. The root locus plot shows that the designed system is stable.

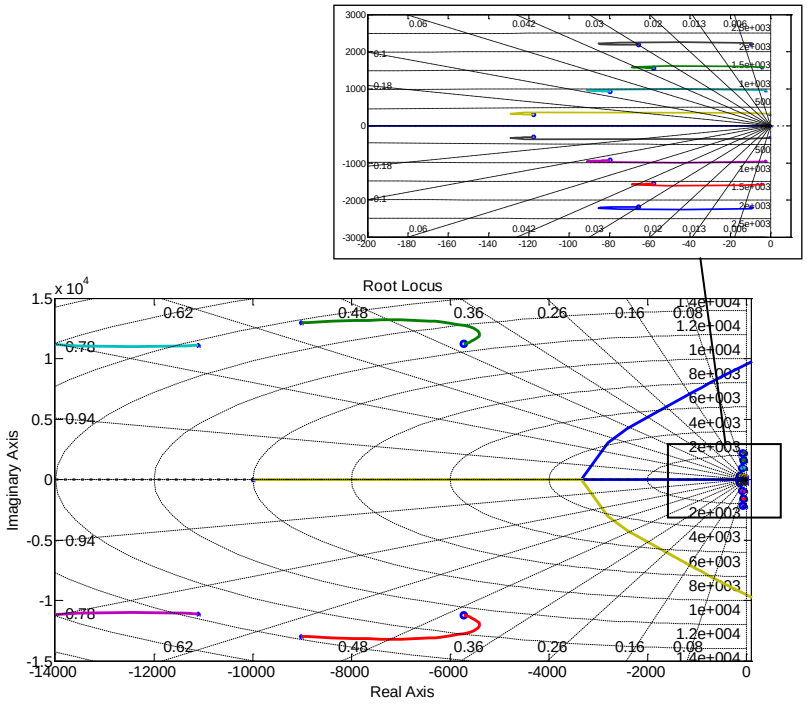

Figure 7. Root Locus of the Inverter with the Fundamental PR Controller and the Harmonic Compensators

Figure 8 and figure 9 show the open loop bode diagram and the closed loop bode diagram of the system, respectively. From the open loop bode diagram, the Gain Margin obtained is 13.2dB at a frequency of 9520rad/s and the Phase Margin obtained is 41.8deg at a frequency of 3310rad/s.

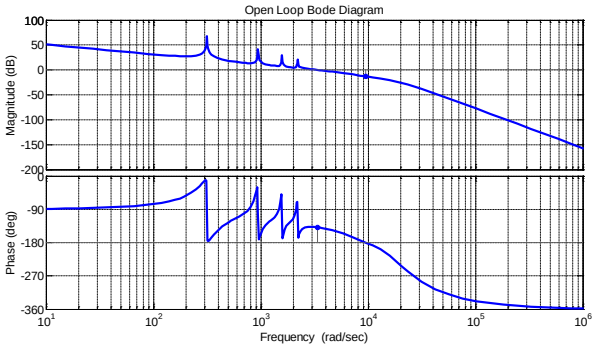

Figure 8. Open Loop Bode Diagram of the System with the Fundamental PR Controller and the Harmonic Compensators

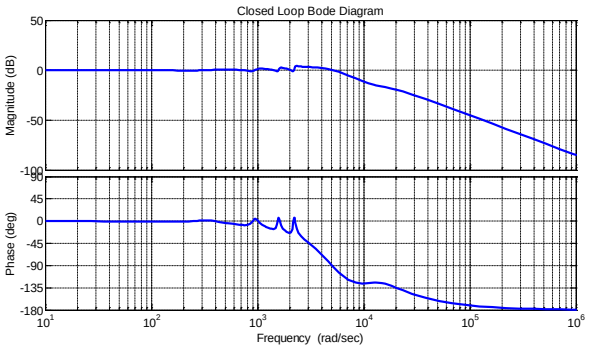

Figure 9. Closed Loop Bode Diagram of the System with the Fundamental PR Controller and the Harmonic Compensators

4. Simulations

The 3kW Grid-Connected PV Inverter was modelled and simulated in Simulink with PLECS blocksets. The grid voltage was set to 325V peak (230V rms), the dc-link voltage was set to 360V and the reference current was set to 18.446A peak to simulate a 3kW inverter. 3rd, 5th and 7th harmonics were added to the grid voltage corresponding to a Total Harmonic Distortion (THD) of 3.37%, to distort the grid voltage sinusoidal waveform. Simulations were carried out to observe the effect of the harmonics with and without harmonic compensation on the inverter voltage and grid current.

Figure 10 and figure 11 show the inverter voltage (V_{pwm}), the grid voltage (V_{grid}), the capacitor voltage (V_{cap}), the inverter current (I_{inv}), the grid current (I_{grid}) and the reference current (I_{ref}) from the simulation in the s-domain using the PR controller without and with harmonic compensation, respectively.

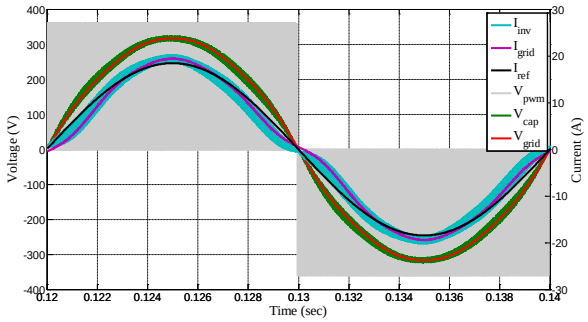

Figure 10. Inverter Operation without Harmonic Compensation (Simulation)

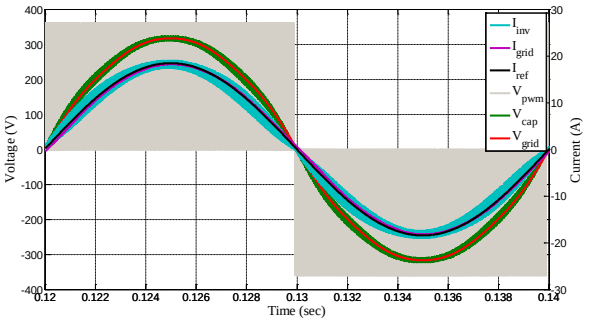

Figure 11. Inverter Operation with Harmonic Compensation (Simulation)

Figure 12 and figure 13 show the harmonic spectrum of the grid current from the simulation using the PR controller without and with harmonic compensation, respectively. From the harmonic spectrum shown in figure 12 it can be seen that the grid current I_{grid} was highly affected by the harmonics present in the grid voltage when no compensation was applied. When considering the harmonics of the grid current as a percentage of the reference current the 3rd, 5th and 7th harmonics were about 8.528%, 3.44% and 1.649%, respectively. When harmonic compensation were applied the 3rd, 5th and 7th harmonics in the grid current I_{grid} were reduced to 0.613%, 0.474% and 0.388%, respectively, as can be observed from figure 13.

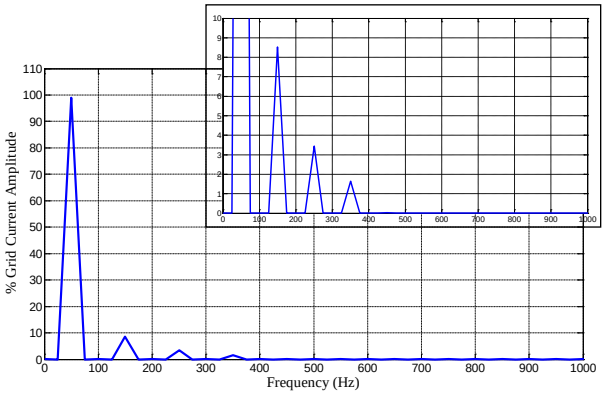

Figure 12. Harmonic Spectrum of the Grid Current without Harmonic Compensation (Simulation)

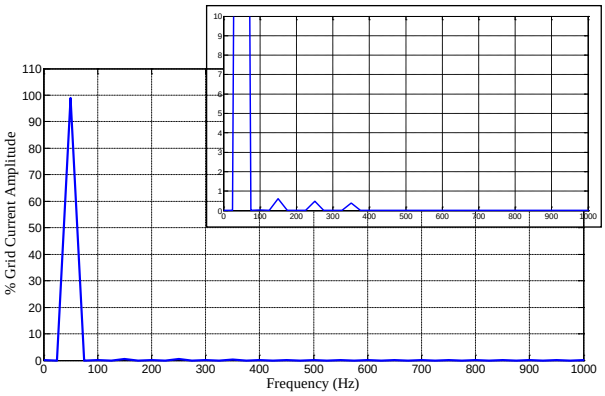

Figure 13. Harmonic Spectrum of the Grid Current with Harmonic Compensation (Simulation)

5. Grid-Connected PV Inverter Testing

The constructed 3kW Grid-Connected PV Inverter test rig is shown in figure 14 below. The inverter was operated at a switching frequency of 10kHz and was connected to a 50Hz grid supply. The inverter was controlled by the dsPIC30F4011 microcontroller from Microchip. Testing was carried out using the PR controller without and with the selective harmonic compensators to analyze the performance of the compensators. The inverter was connected to the grid using a variac to allow variation of the grid voltage for testing purposes. A dc link voltage of 300V was obtained from a dc power supply. The grid voltage was set to 154V rms and the preset reference value of the controller was set to 8A peak.

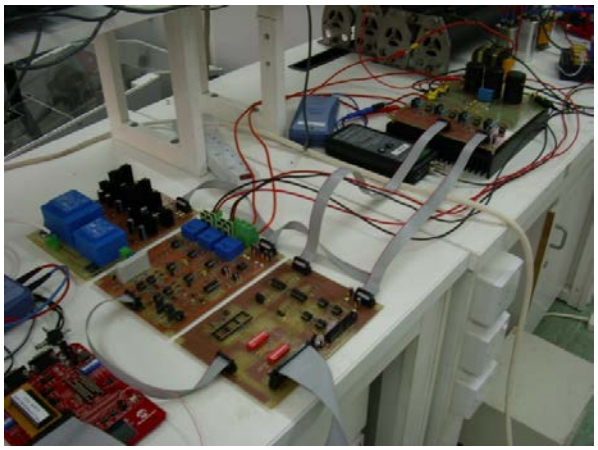

Figure 14. 3kW Grid-Connected PV Inverter Test Rig

Tests were performed to measure the voltage harmonics present in the grid voltage. The 3^{rd}, 5^{th} and 7^{th} harmonics present in the grid voltage were typically about 0.9%, 1.912% and 0.231%, respectively.

Figure 15 and figure 16 show the grid current for the grid-connected inverter with the PR current controller without harmonic compensation and with 3^{rd}, 5^{th} and 7^{th} harmonic compensation, respectively. I_g is the grid current, I_{gr} is the reconstructed grid current up to its 13^{th} harmonic (a reconstruction of the grid current by adding the first 13 lower harmonics) and I_{gfund} is the fundamental component of the grid current.

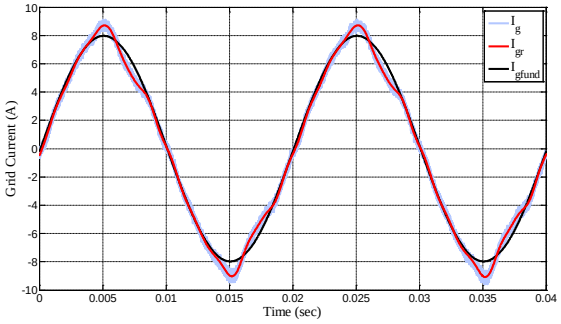

Figure 15. Inverter Grid-Side Current without Harmonic Compensation

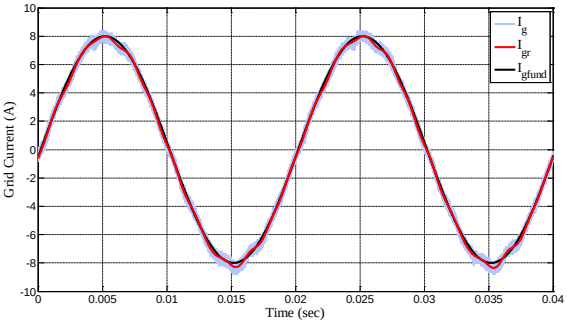

Figure 16. Inverter Grid-Side Current with the 3rd, 5th and 7th Harmonic Compensation

Figure 17 and figure 18 show the harmonic spectrum of the grid current with PR current control without harmonic compensation and with 3rd, 5th and 7th harmonic compensation, respectively. Without harmonic compensation the 3rd, 5th and 7th harmonics resulted about 5.574%, 4.231% and 2.435% of the reference value of 8A peak, respectively. When the harmonic compensators were used the 3rd, 5th and 7th harmonics resulted about 0.378%, 0.641% and 0.24% of the reference value of 8A peak, respectively.

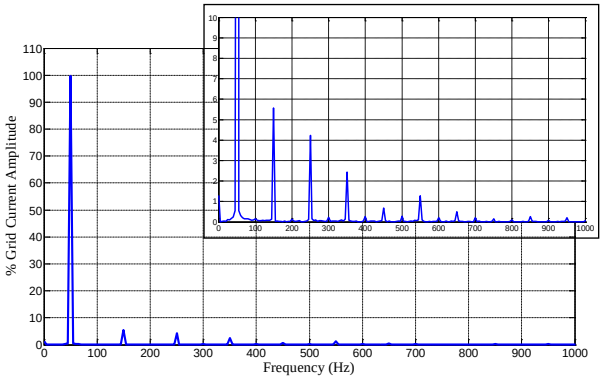

Figure 17. Inverter Grid-Side Current Harmonic Spectrum without Harmonic Compensation

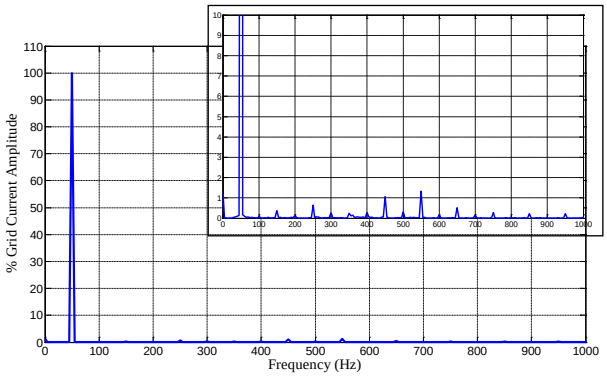

Figure 18. Inverter Grid-Side Current Harmonic Spectrum with the 3rd, 5th and 7th Harmonic Compensators

6. Comparison of Experimental Results

Table 1
Fundamental and Harmonics for the PR Current Controlled Grid-Connected Inverter with Selective Harmonic Compensation

	I_g (Fund.)	I_g (3rd Harm.)	I_g (5th Harm.)	I_g (7th Harm.)
Fund. PR, no compensation	100 %	5.574 %	4.231 %	2.435 %
Fund. PR, 3rd, 5th, 7th Harm. compensation	100 %	0.378 %	0.641 %	0.24 %

The 3rd, 5th and 7th harmonics in the grid voltage were typically about 0.9%, 1.912% and 0.231%, respectively. Table 1 shows the percentage fundamental and harmonic content of the grid current for the PR current controlled grid-connected inverter without and with the selective harmonic compensators. The percentage calculations for the grid current are based on the reference current of 8A peak. The experimental results show the harmonic compensators drastically reduced the 3rd, 5th and 7th harmonics in the grid current. The IEEE 929 and IEEE 1547 standards allow a limit of 4% for each

harmonic from 3rd to 9th and 2% for 11th to 15th [1], [2]. The IEC 61727 standard specifies similar limits [3]. As can be observed from the results obtained the 3rd and 5th harmonics were above the limit when no harmonic compensation was applied. These harmonics result from the inverter non-linearities and also from the harmonics already present in the grid supply. The harmonic compensators reduced the 3rd and 5th harmonics within the limits and reduced further the 7th harmonic, thus making the inverter compliant to the standard regulations.

7. Conclusion

This paper dealt with the reduction of current harmonics generated by grid-connected inverters to make the inverter complaint to the standard regulations. The procedure to design a Proportional Resonant (PR) current controller with additional selective harmonic compensators was presented. Results from simulations as well as from experimental tests were presented and analysed, which showed the effectiveness of the harmonic compensation technique to reduce the current harmonics in the grid current. Experimental testing was carried out on a 3kW Grid-Connected Photovoltaic (PV) Inverter which was designed and built for this research. The 3rd, 5th and 7th harmonics in the grid current were reduced from about 5.574%, 4.231% and 2.435%, respectively, to about 0.378%, 0.641% and 0.24%, respectively, thus making the grid-connected inverter compliant to the IEEE and IEC standard regulations.

References

[1] IEEE 929 2000 Recommended Practice for Utility Interface of Photovoltaic (PV) Systems.
[2] IEEE 1547 Standard for Interconnecting Distributed Resources with Electric Power Systems.
[3] IEC 61727 2004 Standard Photovoltaic (PV) Systems – Characteristics of the Utility Interface.
[4] R. Teodorescu, F. Blaabjerg, U. Borup, M. Liserre, “A New Control Structure for Grid-Connected LCL PV Inverters with Zero Steady-State Error and Selective Harmonic Compensation”, APEC’04 Nineteenth Annual IEEE Conference, California, 2004.
[5] M. Liserre, R. Teodorescu, Z. Chen, “Grid Converters and their Control in Distributed Power Generation Systems”, IECON 2005 Tutorial, 2005.
[6] M. Ciobotaru, R. Teodorescu, F. Blaabjerg, “Control of a Single-Phase PV Inverter”, EPE2005, Dresden, 2005.
[7] D. N. Zmood, D. G. Holmes, “Stationary Frame Current Regulation of PWM Inverters with Zero Steady-State Error”, IEEE Transactions on Power Electronics, Vol. 18, No. 3, May 2003.
[8] D. Zammit, C. Spiteri Staines, M. Apap, “Comparison between PI and PR Current Controllers in Grid Connected PV Inverters”, WASET, International Journal of Electrical, Electronic Science and Engineering, Vol. 8, No. 2, 2014.
[9] R. Teodorescu, F. Blaabjerg, M. Liserre, P. C. Loh, “Proportional-Resonant Controllers and Filters for Grid-Connected Voltage-Source Converters”, IEEE Proc. Electr. Power Appl, Vol. 153, No. 5, 2006.
[10] M. Castilla, J. Miret, J. Matas, L. G. de Vicuna, J. M. Guerrero, “Control Design Guidelines for Single-Phase Grid-Connected Photovoltaic Inverters with Damped Resonant Harmonic Compensators”, IEEE Transactions on Industrial Power Electronics, Vol. 56, No. 11, 2009.
[11] D. Zammit, C. Spiteri Staines, M. Apap, “PR Current Control with Harmonic Compensation in Grid Connected PV Inverters”, WASET, International Journal of Electrical, Computer, Electronics and Communication Engineering, Vol. 8, No. 11, 2014.
[12] V. Pradeep, A. Kolwalkar, R. Teichmann, “Optimized Filter Design for IEEE 519 Compliant Grid Connected Inverters”, IICPE 2004, Mumbai, India, 2004.
[13] R. Teodorescu, M. Liserre, P. Rodriguez, “Grid Converters for Photovoltaic and Wind Power Systems”, Wiley, 2011.
[14] M. Liserre, F. Blaabjerg, S. Hansen, “Design and Control of an LCL-Filter Based Three Phase Active Rectifier”, IEEE Transactions on Industry Applications, Vol 41, No. 5, Sept/Oct 2005.